AIAA JOURNAL
Vol. 39, No. 3, March 2001

Micro-Shock Waves Generated Inside a Fluid Jet Impinging on Plane Wall

G. Jagadeesh,* O. Onodera,† T. Ogawa,‡ and K.Takayama§
Tohoku University, Sendai 980-8577, Japan
and
Z. Jiang¶
Chinese Academy of Sciences, 100080 Beijing, People's Republic of China

An Nd:glass laser pulse (18 ns, 1.38 J) is focused in a tiny area of about 100-μm diam under ambient conditions to produce micro-shock waves. The laser is focused above a planar surface with a typical standoff distance of about 4 mm. The laser energy is focused inside a supersonic circular jet of carbon dioxide gas produced by a nozzle with internal diameter of 2.9 mm and external diameter of 8 mm. Nominal value of the Mach number of the jet is around 2 with the corresponding pressure ratio of 7.5 (stagnation pressure/static pressure at the exit of the nozzle). The interaction process of the micro-shock wave generated inside the supersonic jet with the plane wall is investigated using double-pulse holographic interferometry. A strong surface vortex field with subsequent generation of a side jet propagating outward along the plane wall is observed. The interaction of the micro-shock wave with the cellular structure of the supersonic jet does not seem to influence the near surface features of the flowfield. The development of the coherent structures near the nozzle exit due to the upstream propagation of pressure waves seems to be affected by the outward propagating micro-shock wave. Mach reflection is observed when the micro-shock wave interacts with the plane wall at a standoff distance of 4 mm. The Mach stem is slightly deflected, indicating strong boundary-layer and viscous effects near the wall. The interaction process is also simulated numerically using an axisymmetric transient laminar Navier–Stokes solver. Qualitative agreement between experimental and numerical results is good.

Introduction

SPHERICAL micro-shock waves are produced in the laboratory by focusing an Nd:glass laser pulse (BMI Company, Ltd.) in free air under ambient conditions. The amount of energy expended for producing these tiny shock waves is 1.38 J as measured using a standard laser energy meter. This is equivalent to 0.3 mg of conventional TNT explosive. Considering the amount of energy required for the production of these shock waves, they deserve to be classified as micro-shock waves. The present study focuses on visualizing and understanding the complex interaction process of a micro-shock wave generated inside a circular cross section supersonic carbon dioxide jet impinging on a planar surface. The study is relevant in the background of numerous medical and industrial applications of micro-shock waves.

Explosive-induced spherical underwater shock waves have been successfully used for extracorporeal shock wave lithotripsy.[1] Laser ablation, which is a dry photographic etching technique with submicrometer feature resolution and the ability to remove material in submicrometer layers, is exhaustively used in photographic etching of polymers for lithographic applications.[2] With the ever-shrinking size of micro-electronic devices, laser-assisted techniques[3] are increasingly being integrated with the manufacturing cluster tools in industry. Recent studies on the laser ablation of biological tissues and synthetic polymers such as polymethyl methacrylate (PMMA), polymide, and polyethylene–terephthalate (PET) has led to a new phenomenon called ablative photographic decomposition, which results in ejection of ablated material at supersonic velocities.[4] In most of these applications, shock waves are produced either by exploding microexplosives ranging from a few micrograms to several milligrams[1] or by focusing a laser pulse in a very narrow area of, for example, a few tens of micrometers in diameter.[5]

However, the propagation dynamics of a spherical micro-shock wave is quite complex and is even more intricate when it interacts with stationary obstacles. When micro-shock waves impinge on a wall, depending on the strength and the local intersecting angle with wall, either regular or Mach reflections[6] of the shock wave takes place. The Mach reflection is typically nonlinear in nature with the formation of a triple point, where a slip line and three shock waves merge. Subsequently the slip line, which is a shear layer, transforms itself into a mixing layer away from the triple point, eventually turning into a vortex. Whereas there have been numerous studies on such shock reflection phenomena, the formation, propagation, and reflection dynamics of micro-shock waves are still unclear. The situation becomes cumbersome if the spherical shock wave is intentionally generated inside a fluid jet. In areas such as tissue damage problems in shock-wave-assisted extracorporeal lithotripsy[1] or optical damage due to the blast wave generation[7] in laser-assisted techniques in the microelectronic industry, there is a strong need to understand the basic fluid dynamic behavior of micro-shock waves, as well as in their interaction with supersonic jets. Some aspects of generation, propagation, and reflection of micro-shock waves from a plane wall have been clarified recently by Jiang et al.[8] The presence of secondary imploding shock waves in micro-air blasts produced by pulsed laser focusing has been confirmed recently by Jagadeesh et al.[9]

The main objective of the present study is to visualize qualitatively the complex micro-shock-wave interaction process with the planar obstacle in the presence of a supersonic carbon dioxide jet. Numerical transient simulations are also carried out to understand and verify the experimental results. Double-pulse holographic interferometry is used in this experimental investigation. Numerical interferograms obtained from Navier–Stokes (N–S) simulations compare well with the experimental results. The details of the experimental and numerical study are elucidated followed by a discussion on the important observations of the study.

Received 1 November 1999; presented as Paper 2000-0934 at the AIAA 38th Aerospace Sciences Meeting, Reno, NV, 10–13 January 2000; revision received 10 May 2000; accepted for publication 8 September 2000.

*Visiting Lecturer, Shock Wave Research Center, Institute of Fluid Science. Member AIAA.

†Lecturer, Shock Wave Research Center, Institute of Fluid Science.

‡Technician, Shock Wave Research Center, Institute of Fluid Science.

§Professor, Shock Wave Research Center, Institute of Fluid Science. Member AIAA.

¶Professor, Institute of Mechanics.

Experiments

Focusing of a coherent laser beam readily produces a very high-energy concentration at a peak power density of over several 100 GW/cm^2, resulting in the breakdown of air.[5] The threshold value of focused laser beam intensity for creating breakdown in gases at optical frequencies is proportional to $(Iw^2)/(tp_0)$, where I is the ionization potential, w is the frequency of laser radiation, t is the duration of laser pulse, and p_0 is the initial gas pressure.[10] Once the energy of the focused laser beam exceeds this value, ambient air breaks down with subsequent formation of laser plasma. This in turn generates an outward propagating blast wave. In the present study, a pulsed Nd:glass laser (BMI Company, Ltd.) beam with 18-ns pulse duration is focused in a very minute spot of 100-μm diam, creating micro-air blasts under ambient conditions.

The energy deposition immediately creates a primary spherical micro-shock wave traveling outward from the focal point. This microblast takes a slightly elliptic shape at the very beginning, but quickly transforms into spherical shape within 2–3 μs. Because the energy in the laser pulse is finite, the primary micro-shock-wave velocity decays with the elapse of time, finally becoming a Mach wave. At the same time, inside the laser plasma, rarefaction waves travel toward the point of energy deposition decreasing the density and pressure around the center of the plasma. Subsequently, the flow near the center is overexpanded resulting in the formation of an imploding secondary shock wave.[9]

Figure 1 schematically shows the arrangement used in the experimental investigations. The Nd:glass laser system with a beam diameter of 12 mm has been expanded to 25-mm diam using a combination of concave and convex lenses. The expanded beam is then focused into a spot using an achromatic lens of 70 mm focal length. A double-pulse holographic laser (Apollo Laser, Ltd., Model 22HD) with a pulse width of 25 ns and 2 J of energy per pulse with 694.3 mm wavelength is used for quantitative flow visualization in the experiments. The jet flow from the nozzle is established, which in turn impinges on the plane wall. When the jet flow reaches quasi-steady state, the laser pulse is focused inside the jet for producing the spherical micro-shock wave. Before starting the experiment, the power supply of the laser is switched on for about 5 min for initial charging of the device. The supersonic circular jet of carbon dioxide gas is produced by a nozzle with internal diameter of 2.9 mm and external diameter of 8 mm. Nominal value of the Mach number of the jet is around 2 with corresponding pressure ratio of 7.5 (stagnation pressure/static pressure at the exit of the nozzle). The carbon dioxide gas is fed to the nozzle from a pressure vessel with a provision to measure the pressure close to the inlet of the nozzle.

Initially an argon subsonic jet was used in the experiments. However, considerable difficulties were experienced in visualizing the argon subsonic jet. Hence, to understand the effect of external fluid jet on the fluid dynamic behavior of the micro-shock wave, further experiments were carried out with a supersonic carbon dioxide jet. The refractive index of carbon dioxide is larger than argon, and hence, the gasdynamic features will be clearer in the interferograms. Suitable mechanical fixtures are incorporated in the experimental setup, which facilitate the positioning of the nozzle at desired distances above the planar surface. The planar surface, measuring $96 \times 60 \times 10$ mm, is rigidly fixed on a rigid magnetic housing, and the mounting table has the provision for movement in all three principal axes. In all of the experiments, the standoff distance between the plane wall and the focal point of laser energy deposition is fixed at 4 mm. This distance is chosen based on the minimum standoff distance for the micro-shock wave to reflect back from the surface as a Mach reflection, which is determined from experiments. Two different sets of experiments with the distance between the nozzle outlet and plane wall of 30 and 24 mm are carried out.

Transient axisymmetric N–S numerical analysis is also carried out for comparison with the experimental results. For the computational study, only laminar flow conditions near the wall boundary has been considered treating the micro-shock wave production as an instantaneous energy release from a point source.

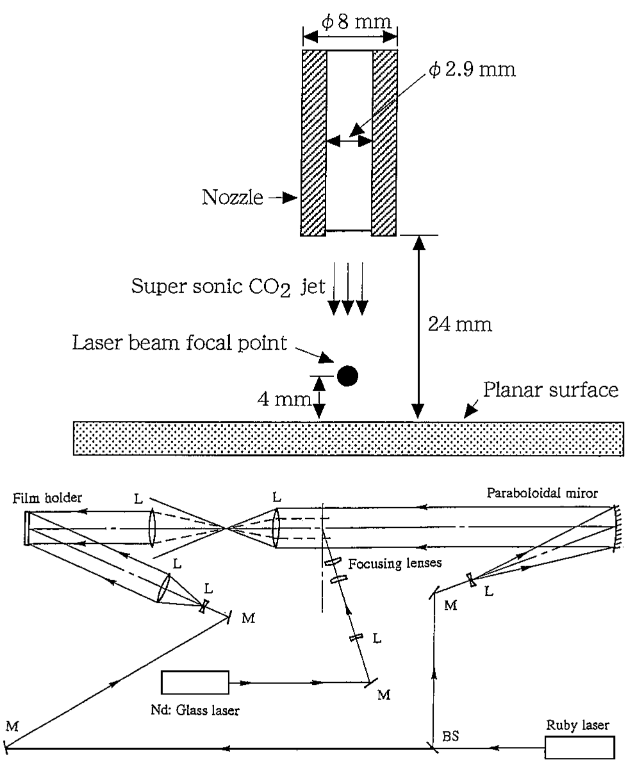

Fig. 1 Schematic diagram of the experimental setup used for generating micro-shock waves and flow visualization.

Numerical Study

Governing Equations

To determine the gasdynamics in the intermediate and far field of microblasts induced by pulsed laser focusing, the random perturbations both in the background and in the inflow conditions are neglected, and the flows are assumed to be axisymmetric in the simulations. The hyperbolic system of the conservation laws, assuming perfect gas, can be written as

$$\frac{\partial U}{\partial t} + \frac{\partial F}{\partial x} + \frac{\partial G}{\partial r} + \frac{1}{r}S = \frac{1}{Re}\left(\frac{\partial R}{\partial x} + \frac{\partial Q}{\partial r} + \frac{1}{r}E\right) \tag{1a}$$

where U, F, G, and S are the state variable, the fluxes in x and r directions, and the source, respectively. They are given by

$$U = \begin{bmatrix} \rho \\ \rho u \\ \rho v \\ e \end{bmatrix}, \qquad F = \begin{bmatrix} \rho \\ \rho u^2 + p \\ \rho u v \\ (e+p)u \end{bmatrix}$$

$$G = \begin{bmatrix} \rho \\ \rho u v \\ \rho v^2 + p \\ (e+p)v \end{bmatrix}, \qquad S = \begin{bmatrix} \rho v \\ \rho u v \\ \rho v^2 \\ (e+p)v \end{bmatrix}$$

$$R = \begin{bmatrix} 0 \\ \tau_{xx} \\ \tau_{xr} \\ u\tau_{xx} + v\tau_{xr} + [\mu/Pr(\gamma-1)]T_X \end{bmatrix}$$

$$E = \begin{bmatrix} 0 \\ \tau_{xr} \\ \tau_{rr} - \tau_{tt} \\ u\tau_{xr} + v\tau_{rr} + [\mu/Pr(\gamma-1)]T_r \end{bmatrix} \tag{1b}$$

with

$$\tau_{xx} = \mu_c\left[\tfrac{4}{3}u_x - \tfrac{2}{3}v_r - (2/3r)v\right], \qquad \tau_{xr} = \mu_c(u_x + v_r)$$

$$\tau_{rr} = \mu_c\left[\tfrac{4}{3}v_r - \tfrac{2}{3}u_x - (2/3r)v\right], \qquad \tau_{rr} - \tau_{tt} = \mu_c[v_r - (v/r)] \tag{1c}$$

where

$$\mu_c = \tfrac{4}{3}\mu + \lambda \tag{1d}$$

Primitive variables in the unknown U are the density ρ, velocity components u and v, and total energy per unit volume e, and p is the fluid pressure. R, Q, and E are the dissipation terms. The equation of state for the perfect gas is given by

$$p = (\gamma - 1)\left\{e - \tfrac{1}{2}\rho(u^2 + v^2)\right\} \tag{2}$$

where γ is the specific heat ratio, taken as 1.3.

The coefficients of viscosity and thermal conductivity have been related to the thermodynamic variables using kinetic theory. Sutherland's normalized formula for viscosity has been used for the viscosity computation.

Numerical Methods

The finite difference equations of Eqs. (1) are discretized using the dispersion-controlled scheme[11] in the form of a half discretization

$$\left(\frac{\partial U}{\partial t}\right)_{ij}^{n} = -\frac{1}{\Delta x}\left(H^n_{i+\frac{1}{2}j} - H^n_{i-\frac{1}{2}j}\right) - \frac{1}{\Delta r}\left(P^n_{i,j+\frac{1}{2}} - P^n_{i,j-\frac{1}{2}}\right)$$

$$-\frac{1}{r}S^n_{i,j} + \frac{1}{Re}\left(\delta^0 R^n + \delta^0 Q^n + \frac{1}{r}E^n\right) \tag{3}$$

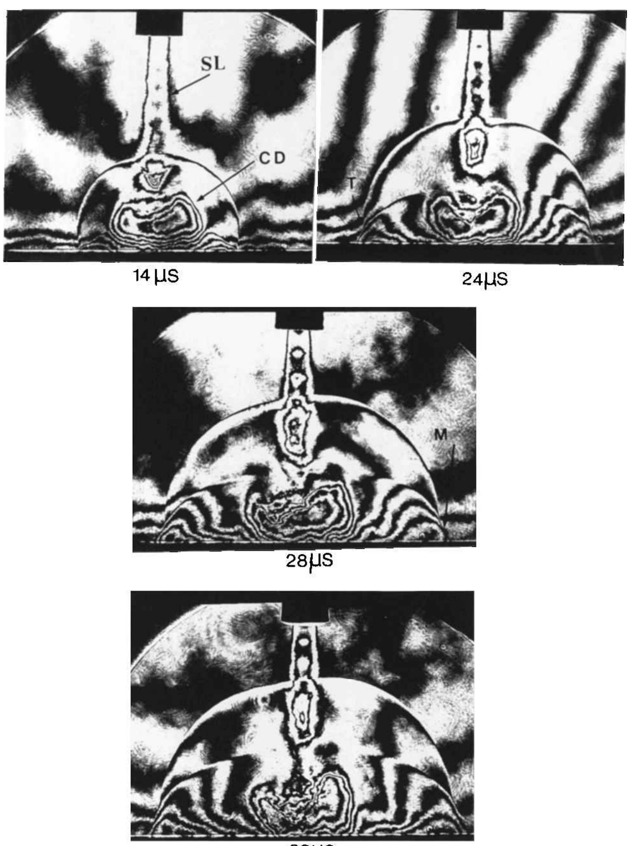

Fig. 2 Interferograms of the visualized flowfield at different time instants; distance between the nozzle exit and planar surface is 30 mm: SL, jet shear layer; CD, contact discontinuity; T, triple point; and M, Mach stem.

where

$$H^n_{i+\frac{1}{2}j} = F^+_{i+\frac{1}{2}L,j} + F^-_{i+\frac{1}{2}R,j}, \qquad P^n_{i,j+\frac{1}{2}} = G^+_{i,j+\frac{1}{2}L} + G^-_{i,j+\frac{1}{2}R} \tag{4}$$

$$F^+_{i+\frac{1}{2}L,j} = F^+_{i,j} + \tfrac{1}{2}\phi^+_A \min\bmod\left(\Delta F^+_{i-\frac{1}{2},j}, \Delta F^+_{i+\frac{1}{2},j}\right)$$

$$F^-_{i+\frac{1}{2}R,j} = F^-_{i,j} - \tfrac{1}{2}\phi^-_A \min\bmod\left(\Delta F^-_{i+\frac{1}{2},j}, \Delta F^-_{i+\frac{3}{2},j}\right) \tag{5}$$

$$G^+_{i,j+\frac{1}{2}L} = G^+_{i,j} + \tfrac{1}{2}\phi^+_B \min\bmod\left(\Delta G^+_{i,j-\frac{1}{2}}, \Delta G^+_{i,j+\frac{1}{2}}\right)$$

$$G^-_{i,j+\frac{1}{2}R} = G^-_{i,j+1} - \tfrac{1}{2}\phi^-_B \min\bmod\left(\Delta G^-_{i,j+\frac{1}{2}}, \Delta G^-_{i,j+\frac{3}{2}}\right) \tag{6}$$

$$\Delta F^{\pm}_{i+\frac{1}{2},j} = \Delta F^{\pm}_{i+1,j} - \Delta F^{\pm}_{i,j}, \qquad \Delta G^{\pm}_{i,j+\frac{1}{2}} = \Delta G^{\pm}_{i,j+1} - \Delta G^{\pm}_{i,j} \tag{7}$$

$$F^{\pm} = A^{\pm}U, \qquad G^{\pm} = B^{\pm}U \tag{8}$$

$$\Phi^{\pm}_A = \boldsymbol{I} \mp \beta\Lambda^{\pm}_A, \qquad \phi^{\pm}_B = \boldsymbol{I} \mp \beta\Lambda^{\pm}_B \tag{9}$$

where δ^0 denotes second-order central differencing. This scheme is designed to meet the dispersion conditions. In the preceding equations, plus or minus superscripts denote vector flux splitting according to the Steger and Warming method. The time-marching integration is performed using a second-order Runge–Kutta scheme. $\boldsymbol{I}$ is a unit vector, $\beta = \Delta t/\Delta x$, and Λ_A and Λ_B are the vectors that

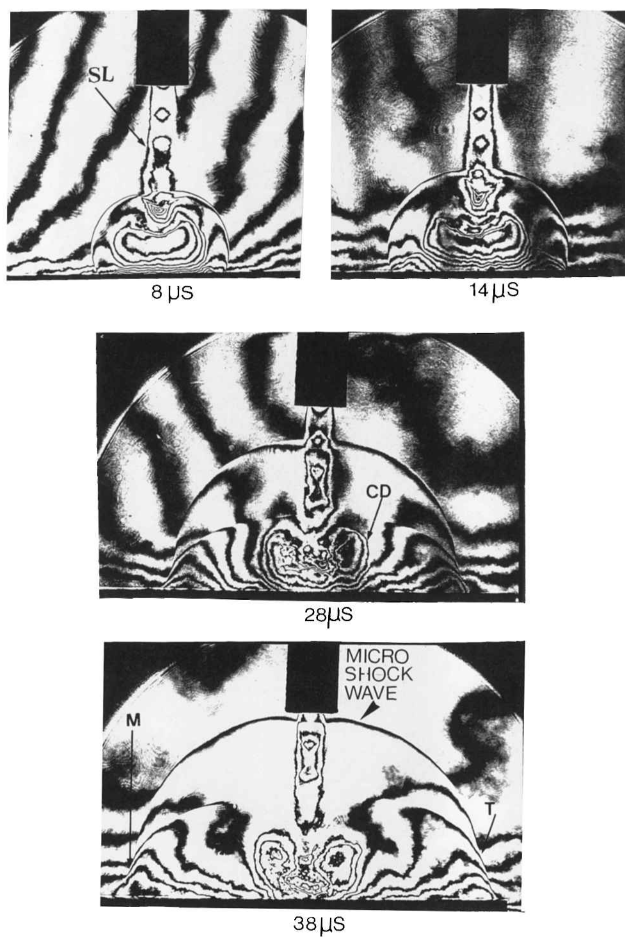

Fig. 3 Interferograms of the visualized flowfield at different time instants; distance between the nozzle exit and planar surface is 24 mm: SL, jet shear layer; CD, contact discontinuity; T, triple point; and M, Mach stem.

consist of the eigenvalues of the matrices A and B, respectively. No-slip boundary conditions are specified on the wall, while reflection boundary conditions are used on the axis of symmetry. The scheme is capable of capturing discontinuity without any numerical oscillations and is achieved without any artificial viscosity. This novel feature of the scheme is very useful in highlighting the fine structures of shock-wave interactions, which diffuse easily, in numerical simulations.

When laser beams are focused into a spot of few tens of micrometers in diameter, due to local high-energy concentration, the pressure and temperature generated at the spot become hundreds or thousands of times higher than those of the ambient air. Numerical simulation of such an explosion requires a very fine mesh, but at the same time, the computational procedure will be interrupted as soon as the simulations are started. This is because of the severe numerical oscillations arising from the sharp discontinuities at the wave front under initial conditions. Hence, it is very critical to specify the right type of initial condition for successful numerical simulation. For simulating the blast wave propagation problems, two types of initial conditions are generally used: a point source and an isothermal sphere. A point source of explosion with 1-mm diam releasing 1.38 J of energy instantaneously is assumed in the present simulations.

However, no attempt is made to model the plasma physics and the real gas effects associated with the initiation of microblast because it is beyond the scope of the present investigation. Moreover, the focus of the present study is to predict the intermediate and the far-field wave dynamics associated with micro-shock wave propagation. To avoid the difficulty of high overpressure in the micro-shock-wave front in the initial stage, the numerical simulations are started a few microseconds after the blast initiation, when the temperature drops to slightly lower values. This is accomplished by specifying proper initial conditions.

Experimental Uncertainties and Numerical Accuracy

The repeatability of micro-shock-wave generation is very high because it depends only on the successful generation of Nd:glass laser pulse. Moreover, because both the energy and duration of the laser pulse is constant, the shot-to-shot variation in the shape of the micro-shock wave generated is virtually negligible. However initial calibration tests have to be carried out to synchronize the internal delay times of both the Nd:glass laser and the ruby laser so that the process can be visualized exactly at the desired time. A conservative estimate of uncertainties associated with supersonic jet flow pressure measurements is $\pm 4\%$. This also includes slight variations in stagnation pressure from run to run due to the pressure loss in the duct connecting the pressure vessel with the inlet of the nozzle. In the beginning of the numerical simulations, the overpressure in the wave front of the microblast is underestimated by 9%; 20 μs later, this error decreases to 5%.

Results and Discussion

Figure 2 shows the sequential experimental interferograms showing the interaction of a micro-shock wave with plane wall in the presence of the supersonic carbon dioxide jet. The distance between the nozzle exit and the plane wall is maintained at 30 mm, whereas the standoff distance between the surface and the laser focal point is 4 mm. The presence of a triple point and Mach stem emanating from the surface signifies Mach reflection of the micro-shock wave. The primary micro-shock wave propagating upstream toward the nozzle is virtually unaffected by the jet. However, the shear layer of the jet is totally shattered after the interaction with the shock wave. The

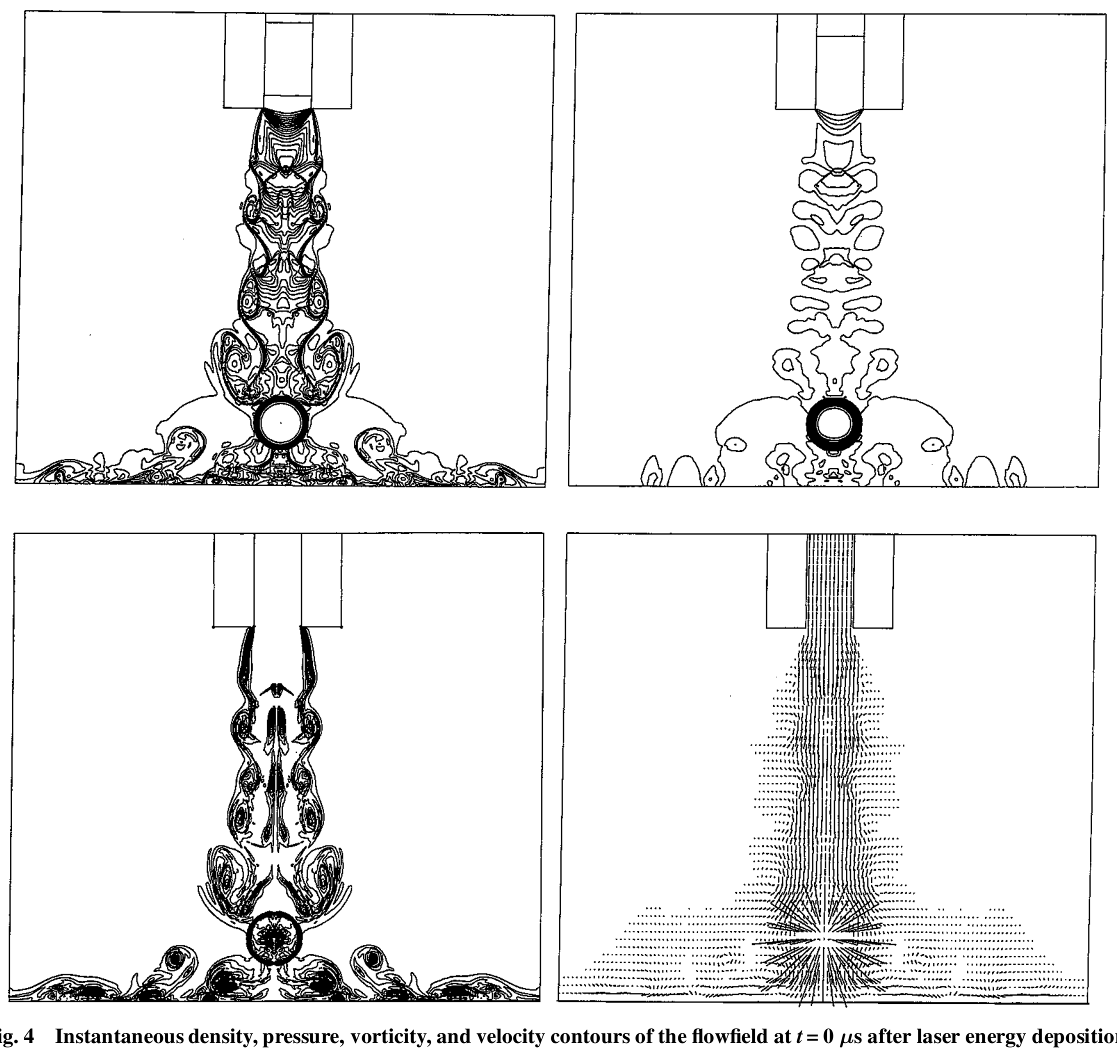

Fig. 4 Instantaneous density, pressure, vorticity, and velocity contours of the flowfield at $t = 0$ μs after laser energy deposition.

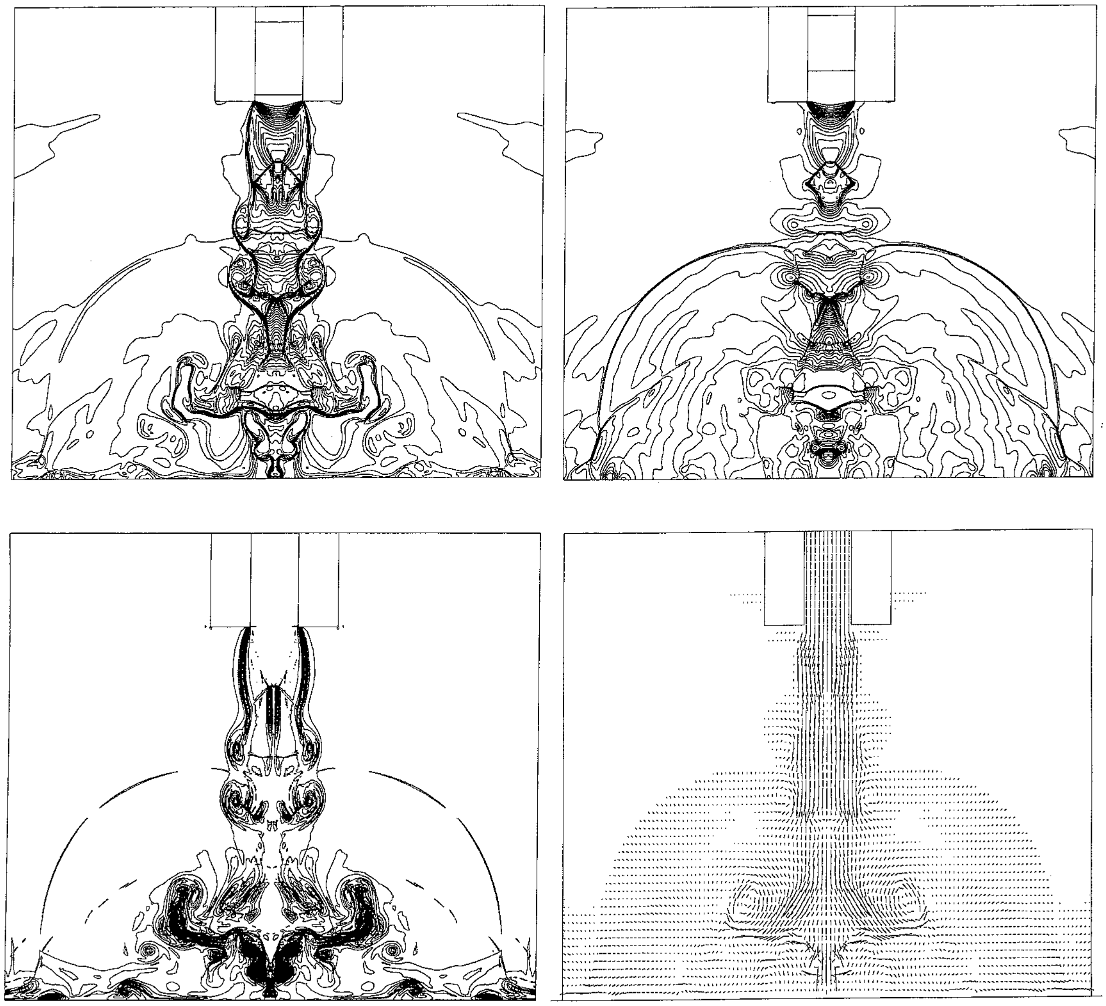

Fig. 5 Instantaneous density, pressure, vorticity, and velocity contours of the flowfield at $t = 28$ μs after laser energy deposition.

contact discontinuity of the micro-shock wave still retains its identity, very close to the stagnation point, but is completely distorted due to the strong kinetic energy transfer from the jet. This interaction also introduces strong near-surface flow instabilities, and the subsequent near-field flow structures appear noncoherent. The upward propagating pressure pulsations due to jet impingement are also noticeable from these interferograms.

Figure 3 shows the sequential interferograms of the flowfield when the distance between the nozzle exit and the planar surface is 24 mm, with identical flow conditions. Even here the primary micro-shock wave appears to be totally unaffected by the interaction with the jet, although slight deflection is noticeable near the nozzle. The contact discontinuity of the micro-air blast seems to be completely shattered, and two lobelike structures are seen. Both the sideward propagating jet and the upward propagating pressure pulsations due to jet impingement are more pronounced in this case. The Mach stem is deflected outward due to the strong surface flow current moving away from the stagnation zone of the planar surface. A strong surface vortex field is also observed from these interferograms.

Because the jet impinges on the plate before the deposition of laser energy in the experiments, the flowfield is three dimensional with perturbations propagating in all of the directions. However axisymmetric transient N–S computations of these phenomena should reproduce the gross flow features observed during experiments. In numerical simulations, the microblast is initiated after the jet reaches quasi-steady-state conditions, and the typical characteristic time of the blast is in microseconds. The computed density, pressure, vorticity, and velocity field immediately after the initiation of the micro-explosion are shown in Fig. 4. In these computations, the standoff distance is 4 mm, while the distance between the nozzle and the surface is 30 mm. Significant flowfield features of a supersonic jet impinging on a plane wall, such as breakdown of the shear layer induced by the upstream propagating pressure waves, development of resulting coherent structure, and impingement of vortex ring on the solid wall, are clearly seen.

Computed flowfield details, 28 μs after laser energy deposition, is shown in Fig. 5. The gross flowfield features observed in the experiments (Figs. 3 and 4) are also captured in the numerical simulations. A strong surface vortex field, Mach stem, shattering of the contact discontinuity, and breakdown of the jet shear layer after interaction with the micro-shock wave are observed from these simulations. To obtain a more qualitative comparison with the experimental results, interferograms and shadowgraphs obtained from the numerical results are shown in Fig. 6a. The effect of microshock interaction with the supersonic jet flowfield is clearly envisaged from Figs. 6. The experimental interferogram corresponding to the same time instant of 28 μs is shown in Fig. 6b. The contact discontinuity of the micro-air blast, which was almost spherical in the absence of the supersonic jet, appears to be the region most affected by the impinging supersonic jet. These near-field instabilities appear to be the result of strong interaction of the jet vortex with the spherical micro-shock wave in the near-field region of the planar surface. Hence, more careful experiments and numerical simulations with higher resolution are needed for resolving these near-surface noncoherent structures. Incorporating an appropriate turbulence model in the axisymmetric transient N–S simulation will also help in further resolving the nonlinear instabilities in the near-wall region. However more accurate modeling of the micro-shock-wave generation by laser plasma, especially in the near field of the blast, will help to obtain an understanding of the breakup process of the contact discontinuity and the characteristics of the nonlinear instabilities. It will also be worthwhile to map accurately the density values of

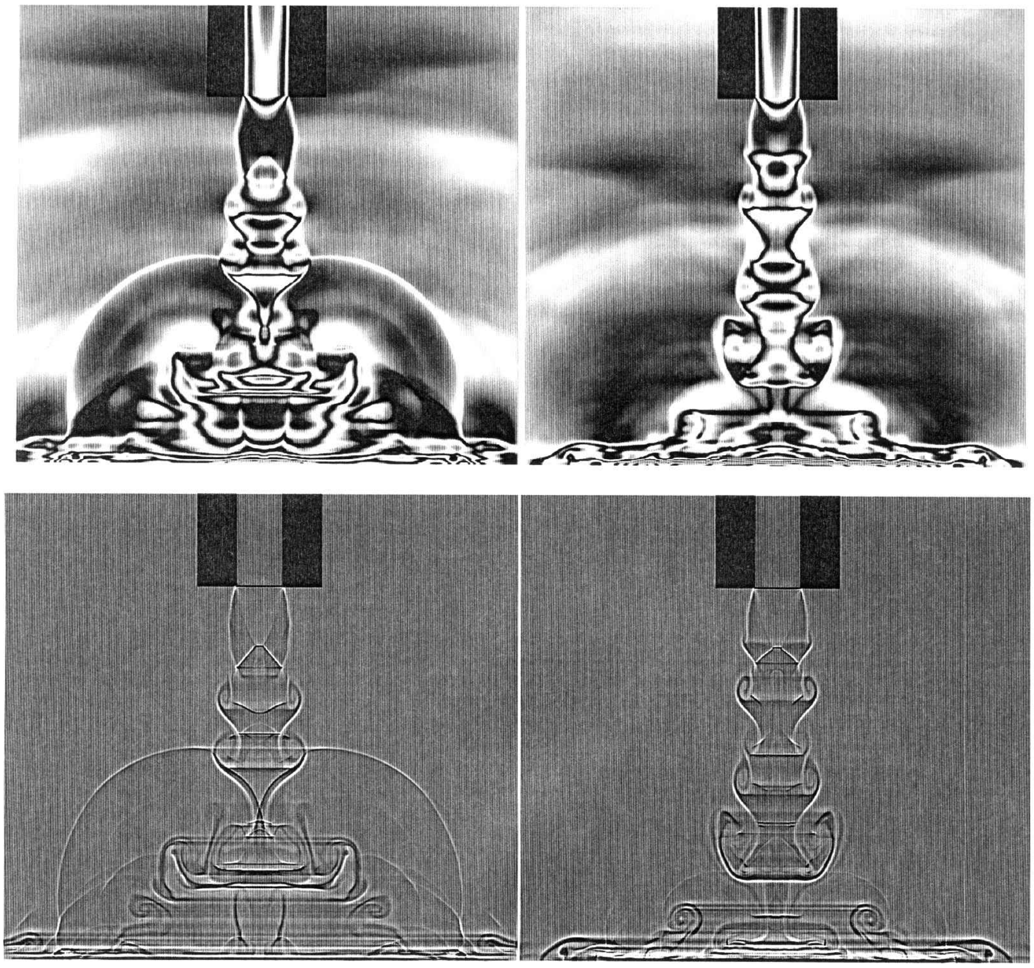

Fig. 6a Numerically simulated interferograms and shadowgraphs of the flowfield: with and without micro-shock wave; $t = 28\ \mu s$.

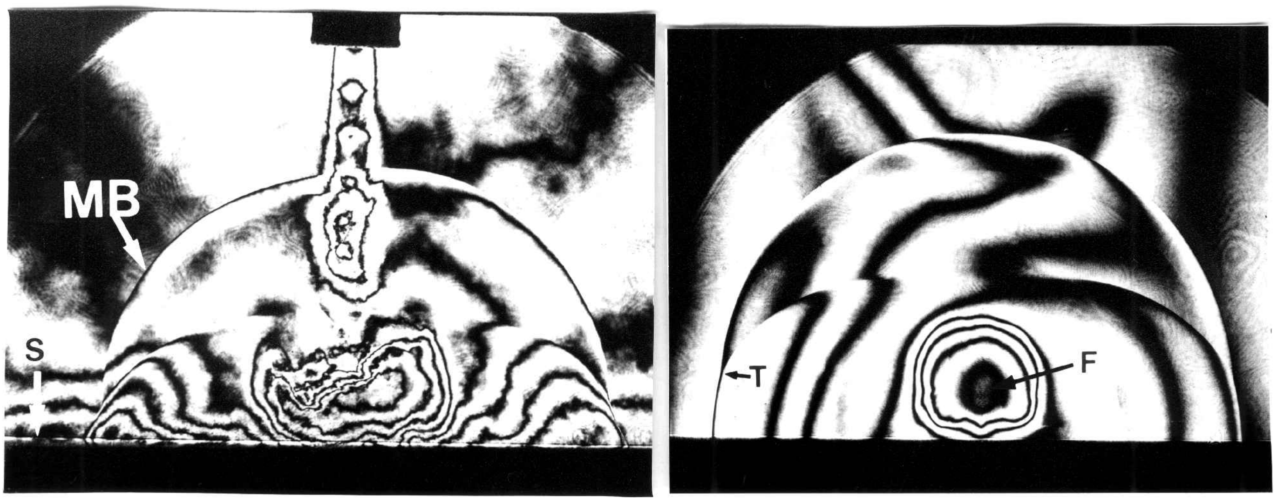

Fig. 6b Experimental interferograms of the flowfield with and without supersonic CO_2 jet; $t = 28\ \mu s$: MB, micro-shock wave; S, planar surface; T, triple point; and F, focal point of energy deposition.

the flowfield using finite fringe interferometry. Experiments are currently underway in the Shock Wave Research Center to determine the density characteristics of the flowfield using finite fringe interferometry coupled with computer-assisted Fourier-transform-based fringe analysis.

Conclusions

The interaction process of a spherical micro-shock wave generated within a supersonic carbon dioxide jet impinging on a planar surface is visualized using double-pulse holographic interferometry. Axisymmetric laminar N–S computations are also carried out to help understand the micro-shock-wave interaction process. The important conclusions of the study are enumerated as follows.

1) The primary micro-shock wave remains unaffected after interacting with the supersonic carbon dioxide jet. However, slight deflection of the shock wave is noticed at a reduced distance between the nozzle exit and the plane wall.

2) Mach reflection of the micro-shock wave is visualized at the standoff distance of 4 mm, and the Mach stem is deflected outward by the side jet produced on the boundary of the wall.

3) Strong nonlinear instabilities are produced close to the surface due to the interaction of the micro-air blast contact discontinuity and the jet.

4) A strong surface vortex field is observed on the planar surface after the interaction process of the jet and the micro-shock wave.

5) Although the upward propagating pressure pulsations due to jet impingement are observed in the flowfield, the shear layer is completely destroyed on interaction with the outward propagating spherical micro-shock wave.

6) However, the shock cell structures seen in the supersonic jet remain unaffected by the primary micro-shock wave.

7) The downstream convected coherent structures from the supersonic jet are noticeable in the flowfield, but they disappear on interacting with the spherical micro-shock wave.

8) In spite of the interaction process, the upstream propagating pressure waves and the coherent structures appear to be phase locked at the nozzle exit.

The enhanced near surface instabilities and the generation of the side jet along with a strong surface vortex field will be useful in utilizing the micro-shock-wave interaction process with a supersonic jet for various surface cleaning applications. Further research is mandatory for the accurate quantification of the various flow variables.

References

[1] Kodama, T., Uenohara, H., and Takayama, K., "Innovative Technology for Tissue Disruption by Explosive-Induced Shock Waves," *Ultrasound in Medicine and Biology*, Vol. 24, No. 9, 1998, pp. 1459–1466.

[2] Zyung, T., Kim, H., Jay, C. P., and Dana, D. D., "Ultra Fast Imaging of 0.532-μm Laser Ablation of Polymers: Time Evolution of Surface Damage and Blast Wave Generation," *Journal of Applied Physics*, Vol. 65, No. 12, 1989, pp. 4548–4563.

[3] Vereecke, G., Rohr, E., and Heyns, M. M., "Laser-Assisted Removal of Particles on Silicon Wafers," *Journal of Applied Physics*, Vol. 85, No. 7, 1999, pp. 3837–3843.

[4] Reddy, K. P. J., "Self-Similar Solutions of Laser Produced Blast Waves," *Pramana—Journal of Physics*, Vol. 46, No. 2, 1996, pp. 153–159.

[5] Sappey, A. D., and Nogar, A. D., "Laser Ablation in Atmosphere," *Laser Ablation*, edited by J. C. Miller, Springer-Verlag, New York, 1994, pp. 166–171.

[6] Ben-Dor, G., "General Introduction," *Reflection of Shock Waves*, Springer-Verlag, New York, 1991, pp.1–36.

[7] Kim, H., Jay, C. P., Zyung, T., and Dana, D. D., "Ultra Fast Imaging of Optical Damage Dynamics and Laser-Produced Wave Propagation in Polymethyl Methacrylate," *Journal of Applied Physics*, Vol. 64, No. 6, 1988, pp. 2955–2958.

[8] Jiang, Z., Takayama, K., Moosad, K. P. B., Onodera, O., and Sun, M., "Numerical and Experimental Study of Micro-Blast Wave Generated by Pulsed-Laser Beam Focusing," *Shock Waves*, Vol. 8, No. 6, 1998, pp. 337–349.

[9] Jagadeesh, G., Toro, E. F., Jiang, Z., Onodera, O., Ogawa, T., and Takayama, K., "Secondary Shock Waves in Micro-Air Blasts Generated by Laser Pulse Focusing," *Shock Waves* (to be published).

[10] Shugaev, F. V., and Shtemenko, L. S., "Laser-Driven Shock Waves," *Propagation and Reflection of Shock Waves*, 1st ed., Vol. 49, Series on Advances in Mathematics for Applied Sciences, World Scientific, Singapore, 1997, pp. 197–212.

[11] Jiang, Z., Takayama, K., and Chen, Y. S., "Dispersion Conditions for Non-Oscillatory Shock Capturing Schemes and its Applications," *Computational Fluid Dynamics Journal*, Vol. 2, No. 4, 1995, pp. 137–150.

M. Sichel
Associate Editor